OXFORD

Social Cognitive and Affective Neuroscience, 2022, **17**, 187–197

DOI: https://doi.org/10.1093/scan/nsab085
Advance Access Publication Date: 9 July 2021
Original Manuscript

A 7-Tesla MRI study of the periaqueductal gray: resting state and task activation under threat

Carissa N. Weis,[1] Kenneth P. Bennett,[2] Ashley A. Huggins,[1] Elizabeth A. Parisi,[1] Stephanie M. Gorka,[3] and Christine Larson[1]

[1]Department of Psychology, University of Wisconsin—Milwaukee, Milwaukee, WI 53211, USA
[2]Montana VA Healthcare System, Helena, MT 59636, USA
[3]Institute for Behavioral Medicine Research, The Ohio State University, Columbus, OH 43210, USA
Correspondence should be addressed to Carissa N. Weis, Department of Psychology, University of Wisconsin – Milwaukee, 2441 E Hartford Ave, Milwaukee, WI 53211, USA. E-mail: cweis@mcw.edu.

Abstract

The periaqueductal gray (PAG) is a region of the midbrain implicated in a variety of behaviors including defensive responses to threat. Despite the wealth of knowledge pertaining to the differential functional roles of the PAG columns in nonhuman and human research, the basic functional connectivity of the PAG at rest has not been well characterized. Therefore, the current study utilized 7-Tesla magnetic resonance imaging (MRI) to characterize PAG functional connectivity at rest and task activation under uncertain threat. A sample of 53 neurologically healthy undergraduate participants ($M_{age} = 22.2$, $s.d._{age} = 3.62$) underwent structural and resting state functional MRI scans. Supporting previous work, voxel-wise analyses showed that the PAG is functionally connected to emotion regulation and fear networks. The comparison of functional connectivity of PAG columns did not reveal any significant differences. Thirty-five participants from the same sample also completed an uncertain threat task with blocks of three conditions—no shock, predictable shock and unpredictable shock. There were no robust activity differences within the PAG columns or the whole PAG across conditions although there was differential activity at the voxel level in the PAG and in other regions theoretically relevant to uncertain threat. Results of this study elucidate PAG connectivity at rest and activation in response to uncertain threat.

Key words: periaqueductal gray; PAG; resting state; functional connectivity; NPU; uncertain threat

Introduction

The periaqueductal gray (PAG) is a region of the midbrain that has been implicated in a variety of complex behaviors including defensive responses to threat, as well as integrating information from multiple systems (i.e. somatic, autonomic and sensory systems) to coordinate and regulate emotional behavior (Fanselow, 1991; Behbehani, 1995; An *et al.*, 1998; Bandler *et al.*, 2000; Lindquist *et al.*, 2012; Motta *et al.*, 2017). Given its role in defensive behaviors, the PAG is a critical region of fear and anxiety neurocircuitry (Fanselow, 1991). Characterizing the basic functional connectivity of the PAG is important to understanding how dysfunction may underlie aberrant fear and anxiety states.

The anatomical connectivity of the PAG has been well characterized in nonhuman animal work (Mantyh, 1983a,b; An *et al.*, 1998; Jansen *et al.*, 1998; Bandler *et al.*, 2000; Krout and Loewy, 2000; Barbaresi and Mensa, 2016). Retrograde tracers injected in the PAG in macaque monkeys show clear connections to medial and ventrolateral prefrontal cortex (PFC), anterior cingulate cortex (ACC), caudal and lateral orbitofrontal cortex, temporal pole, ventral insula, superior temporal sulcus and gyrus, basal forebrain, hypothalamus and amygdala (An *et al.*, 1998). Anterograde tracers injected in the PAG in macaque monkeys show connections to medial PFC, posterior orbital cortex and ACC (An *et al.*, 1998; Bandler *et al.*, 2000). More specifically, strong projections were also shown from medial PFC to the dorsolateral column of the PAG, orbital cortices more strongly projected to the ventrolateral column and cingulate regions were more strongly connected to the lateral column (An *et al.*, 1998; Bandler *et al.*, 2000).

In addition to structural connectivity differences, studies with nonhuman animals have also shown columns of the PAG can be distinguished by differences in cytoarchitecture and neurochemistry (Menant *et al.*, 2016). The columnar organization of the PAG likely underlies the varied functional outcomes elicited in animal models. The dorsal columns have been implicated in active-coping defensive strategies such as fear, panic and fleeing behaviors (Behbehani, 1995; An *et al.*, 1998; Bandler *et al.*, 2000; Molchanov and Guimaraes, 2002; Vianna *et al.*, 2003; Bittencourt *et al.*, 2004; Mendes-Gomes and Nunes-de-souza, 2009; Deng *et al.*, 2016; Motta *et al.*, 2017; Vieira-Rasteli *et al.*, 2018). The lateral PAG columns have also been implicated in active-coping threat reactions (Fanselow, 1991; Bittencourt *et al.*, 2004; Faull *et al.*, 2019). Finally, the ventral columns appear to facilitate

Received: 3 December 2020; **Revised:** 23 June 2021; **Accepted:** 8 July 2021

passive-coping strategies such as freezing or quiescence behaviors (Fanselow, 1991; Behbehani, 1995; An *et al.*, 1998; Bandler *et al.*, 2000; Molchanov and Guimaraes, 2002; Vieira-Rasteli *et al.*, 2018).

In humans, the distinct structural connectivity (Ezra *et al.*, 2015) and functional roles of the PAG columns are also well-maintained although the PAG is less frequently studied due to its inaccessibility (i.e. size and location). Most of the functional connectivity works of the human PAG have examined task-based effects that elicit the differential activity of the PAG columns through a wide variety of task paradigms in the magnetic resonance imaging (MRI) scanner (Mobbs *et al.*, 2007; Hahn *et al.*, 2013; Ritter *et al.*, 2013; Satpute *et al.*, 2013; La Cesa *et al.*, 2014; Faull *et al.*, 2015, 2016; Faull and Pattinson, 2017; Hashemi *et al.*, 2019; Kragel *et al.*, 2019).

Despite all of this, and to the best of authors' knowledge, basic functional connectivity of the PAG and its columns in healthy individuals has only been characterized in two other studies (Coulombe *et al.*, 2016; Faull and Pattinson, 2017). In addition, given its small size, conventional 3-Tesla MRI produces inadequate spatial resolution to distinguish the columns. However, the use of 7-Tesla MRI has demonstrated significantly improved spatial resolution for PAG function as compared to 3T (Hahn *et al.*, 2013). Therefore, the current study utilized high-resolution 7-Tesla MRI to characterize the functional connectivity of the PAG and its columns (ventrolateral, lateral, dorsolateral and dorsomedial) in healthy individuals at rest (Experiment 1). To follow up the resting state analysis, PAG activity was also assessed under an uncertain threat of shock paradigm (Experiment 2).

Experiment 1: resting state functional connectivity of the PAG

Method

Participants

Neurologically healthy undergraduate students from the University of Wisconsin-Milwaukee were recruited to participate in this study ($n = 57$; 12 males, 45 females; $M_{age} = 22.2$, $s.d._{age} = 3.62$; 56% Caucasian, 14% Asian or Pacific Islander, 12% African American, 12% Hispanic and 4% Other). The participants in the current study are part of the same dataset reported in Weis *et al.* (2019). Inclusion criteria included being over 18 years old, right handed and English speaking. Exclusion criteria included history of head trauma, neurologic disorder, history of psychosis or bipolar disorder, current use of antipsychotics, anticonvulsants or mood stabilizers and any contraindications to MRI including metal in the body, pregnancy or claustrophobia. Note that participants were not excluded for medications such as antidepressants or anxiolytics that may have effects on anxiety neurocircuitry including the PAG (Harris and Reynell, 2017). These data were also not recorded as part of this study and, thus, cannot be examined as a potential confound in our results. The University of Wisconsin Milwaukee and the Medical College of Wisconsin Institutional Review Boards approved this study. Participants provided written informed consent, according to the Declaration of Helsinki, and were paid for their participation in the study.

MRI acquisition

Magnetic resonance (MR) images were collected on a 7-Tesla MR950 General Electric scanner with a 32-channel Nova coil. High-resolution axial T1-weighted whole-brain anatomical images were acquired (voxel resolution = 0.43 × 0.43 × 0.80 mm, slice thickness = 0.8 mm, repetition time (TR) = 8.012 ms, echo time = 3.784 ms, inversion time = 1050 ms, flip angle = 5°, field of view = 220 mm, matrix = 276 × 276). A single-shot gradient echo-planar Image (EPI) sequence was used for the 8min resting state scan where participants were instructed to stay awake and blink normally while being shown a white fixation cross on a black background (volumes = 192, repetition time = 2500 ms, echo time = 24 ms, flip angle = 73°, field of view = 220 mm, matrix = 224 × 224, number of excitations = 1, slice thickness = 1.8 mm, 30 axial slices with 0 mm gap, voxel resolution = 0.859 × 0.859 × 1.80 mm). To optimize the spatial resolution advantages of 7T, EPI scans were acquired with partial coverage of the brain. Coverage was determined for each individual participant such that the top of the insula was covered by the most superior slices and the hippocampus covered by the most inferior slices. See Figure 1 for coverage of a representative participant. For distortion correction in the EPI preprocessing, an additional single-volume EPI scan with reverse phase-encoding polarity was collected. The average signal-to-noise ratio = average[signal]/s.d.[noise] calculated in AFNI for the preprocessed functional data after regression across the sample was 120.93.

Resting state fMRI analysis

Freesurfer version 6.0 was used to segment the tissue type for each individual's anatomy (Fischl, 2012). Preprocessing and analysis of the resting state fMRI were performed using the ANATICOR (Jo *et al.*, 2010) processing pipeline in AFNI (version AFNI_19.2.01 'Claudius') (Cox, 1996). ANATICOR is a denoising protocol that removes unwanted signal from white matter and ventricles by using eroded white matter and ventricle masks extracted from FreeSurfer to reduce any partial volume effects in the gray matter signal. Ventricular and white matter signal regressors are estimated before smoothing and projected out of the final functional dataset ahead of correlational analyses.

The first three volumes were removed from the EPI to remove pre-steady-state artifacts. The remaining volumes were despiked and slice time corrected to the first slice. Given the greater sensitivity to distortions at ultra-high field, EPI and reverse polarity scans were warped to a middle space for distortion correction (-plusminus in 3dQwarp). Functional volumes were then co-registered to the first functional volume and aligned to the anatomy (-partial_axial in align_epi_anat.py). The anatomy and EPI were then warped to MNI space (MNI152) for group analysis. Given the close spatial proximity of the PAG columns and to preserve the high-resolution EPI, PAG column time series were extracted prior to smoothing. Functional images were then smoothed with a 3.6 mm kernel (double the functional voxel size) (Satpute *et al.*, 2013).

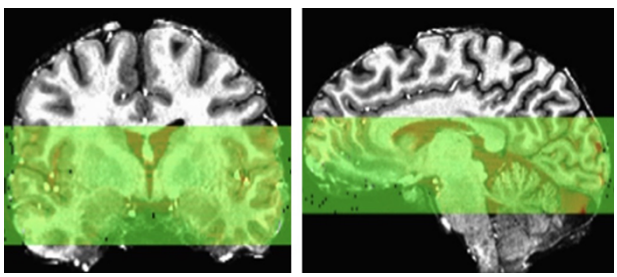

Fig. 1. Depiction of partial EPI acquisition coverage for a representative participant shown in native space.

In the regression (3dDeconvolve), one censor file was included that indicated TRs to exclude where more than 10% of voxels in the brain were outliers and/or where excessive motion yielded a frame-to-frame Euclidean norm motion derivative greater than 0.3 mm (Torrisi *et al.*, 2015; Gorka *et al.*, 2017). Three participants (three females) were dropped from final analysis for exceeding the motion threshold (>15% TRs censored) leaving a final sample of 54. Six head motion parameters and their derivatives, a bandpass filter (0.01–0.1 Hz) and the time series from eroded ventricle and white matter masks were also included as regressors and projected out of the final dataset. The estimated blur of the final EPI dataset was calculated with *3dFWHMx*. To correct for multiple comparisons, resultant average auto-correlation function parameters were entered in *3dClustSim* to determine the voxel-wise $P < 0.001$ and cluster thresholds $P < 0.05$, $k > 303$ (Woo *et al.*, 2014; Chen *et al.*, 2017).

Definition of PAG seeds

Manual segmentation of the PAG was done in reference to Duvernoy's Atlas of the Human Brain Stem and Cerebellum (Duvernoy, 2009) and in accordance with previous human PAG segmentation protocols (Satpute *et al.*, 2013; Kragel *et al.*, 2019). The method employed for manual segmentation involves first determining the placement of the cerebral aqueduct followed by the identification of the surrounding PAG. After carefully reviewing the alignment of the anatomy and EPI images for each participant, it was determined that the manual tracing of the aqueduct and PAG could be done on the anatomical images aligned to standard MNI space rather than the anatomy in the original subject's space. This decision also reduces the need for transformations performed on the PAG masks and ensures resultant masks are well aligned to the high-resolution EPI.

Manual tracing began at the first axial slice where the cerebral aqueduct no longer appeared to be connected to the third ventricle. Tracing continued inferiorly until the last slice where the aqueduct is clearly surrounded by gray matter. From a sagittal view, the aqueduct should be wedged between rostral and caudal gray matter and should not continue into the cavernous 5th ventricle. With a slice thickness of 0.8 mm, in the current dataset, the aqueduct extended ∼15 slices (per the average longitudinal length reported in Satpute *et al.*, 2013). Once the aqueduct was identified, its mask was used to create the PAG by dilating out two voxels in all directions: $+0.86 \times 0.86 \times 1.60$ mm (Satpute *et al.*, 2013; Kragel *et al.*, 2019). Then, the original tracing of the aqueduct was subtracted out from the dilation, leaving only the voxels surrounding it. Resultant PAG masks were visually inspected for placement and alignment to the EPI and manually edited if needed (see Supplementary Figure S1 for further manual segmentation protocol details). AFNI's dilation procedure (in *3dmask_tool*) occurs across the 18 neighbors a given voxel shares either a face or an edge with, i.e. all of the neighbors in a $3 \times 3 \times 3$ box except the eight outer corners. Thus, depending on the initial drawing of the aqueduct, further dilation may extend too far and include voxels (especially at outer corners) likely not belonging to the PAG. Manual editing entailed removing these extraneous voxels and occurred in <25% of the sample. One participant (female) was removed from analysis due to insufficient coverage of the PAG mask, leaving a final sample of 53 (12 males and 41 females).

Since signal from the cerebrospinal fluid (CSF) in the aqueduct can contaminate our intended signal of interest, we wanted to verify voxels of the aqueduct were appropriately removed from PAG masks. To do this, we compared average signal variability between the aqueduct and PAG masks for each participant (Satpute *et al.*, 2013). This comparison demonstrated 10 times greater variability overall in aqueduct signal intensity as compared to PAG and further validates appropriate separation of the noisy CSF versus the gray matter signal of interest (Supplementary Figure S2).

Segmentation of the four columns of the PAG was done one time at the group level. This decision was made to reduce the amount of bias that may result from segmenting the columns separately for each individual subject. Furthermore, there is no established protocol in the literature to segment PAG columns, and although voxel resolution is very high at 7T, it is still not high enough to make judgments on PAG column delineation according to any anatomical features. First, an average group mask of all the individual manually drawn PAG masks was created. Calculation of the Sorenson–Dice coefficient (DSC) across all manually segmented PAG masks indicates imperfect overlap of masks ($DSC = 0.51$). Therefore, the group mask was then thresholded to retain voxels identified as the PAG in at least 50% of the sample. This group mask was visually inspected for accuracy (see Supplementary Figure S3 for group PAG mask overlaid on an average functional scan). Next, the columns of the PAG were segmented on the group mask by dividing the PAG into dorsomedial, bilateral dorsolateral, bilateral lateral, bilateral ventrolateral and ventromedial columns (Ezra *et al.*, 2015). The ventromedial column was segmented to aid in the delineation of the other columns but was not included in further analyses as its thought to be part of other brainstem nuclei (Ezra *et al.*, 2015). Left and right hemispheres were combined for dorsolateral, lateral and ventrolateral columns (Figure 2). Then using this group mask, average time series was extracted for each participant for each of the four columns from the pre-smoothed distortion corrected aligned functional data. Given the size and spatial proximity of the PAG columns, for each participant Pearson correlations for all pairwise PAG column time series were calculated, Fisher Z-transformed, averaged and back-transformed to obtain standardized group 'average correlations' (Supplementary Table S1). Not surprisingly, each pair of columns was highly correlated within individual subjects (Coulombe *et al.*, 2016).

To analyze voxel-wise functional connectivity of the PAG columns, the time series for each column (extracted before smoothing) was correlated with every other voxel within the field of view and resulting correlation maps were r-to-z transformed. However, to account for the high degree of correlation among columns, a repeated measure analysis of covariance (ANCOVA) using AFNI's *3dMVM* was performed with PAG column as a repeated measure (Chen *et al.*, 2014; Coulombe *et al.*, 2016). With a greater number of females in the sample, sex was included as a covariate in the model. For each PAG column, correlations between average seed time series (before smoothing) and the time series of every other voxel within the field of view were calculated while controlling for the effects of the other three columns of interest. See Supplementary Table S2 for *3dMVM* command.

Results

Resting state results

Whole PAG functional connectivity First, voxel-wise connectivity of the *whole PAG* seed manually drawn for each participant was assessed. Results of the whole PAG seed analysis show surviving clusters were in theoretically expected regions (Figure 3). For instance, the PAG showed significant connectivity with anterior cingulate, superior orbital and hippocampal cortices, insula

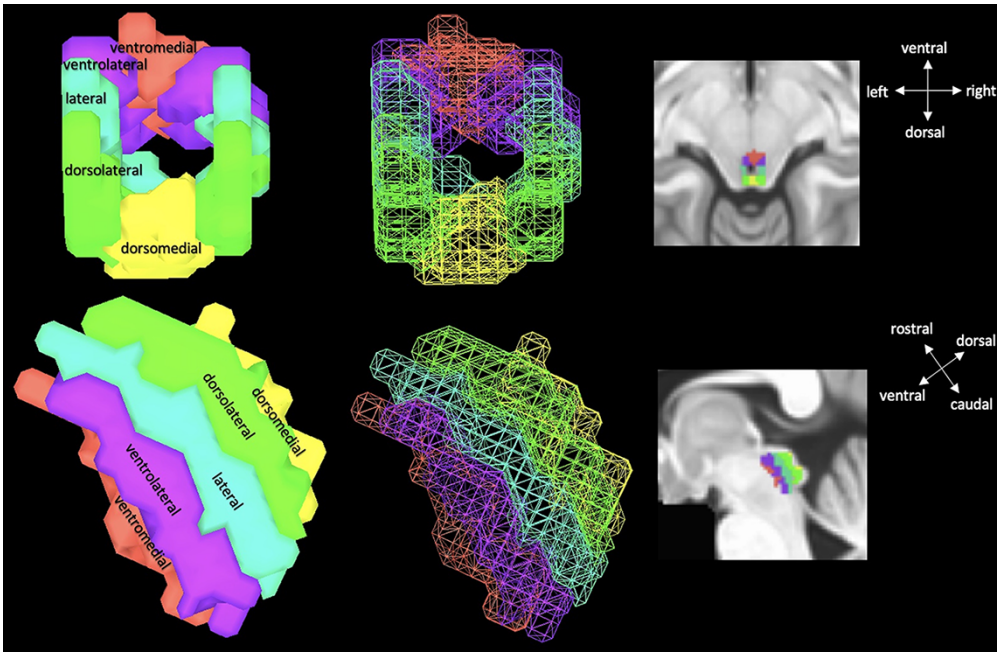

Fig. 2. Illustration of group level unsmoothed PAG seed with columns—ventromedial (red), ventrolateral (purple), lateral (teal), dorsolateral (lime green) and dorsomedial (yellow). Note that the ventromedial region was segmented but not used in analysis.

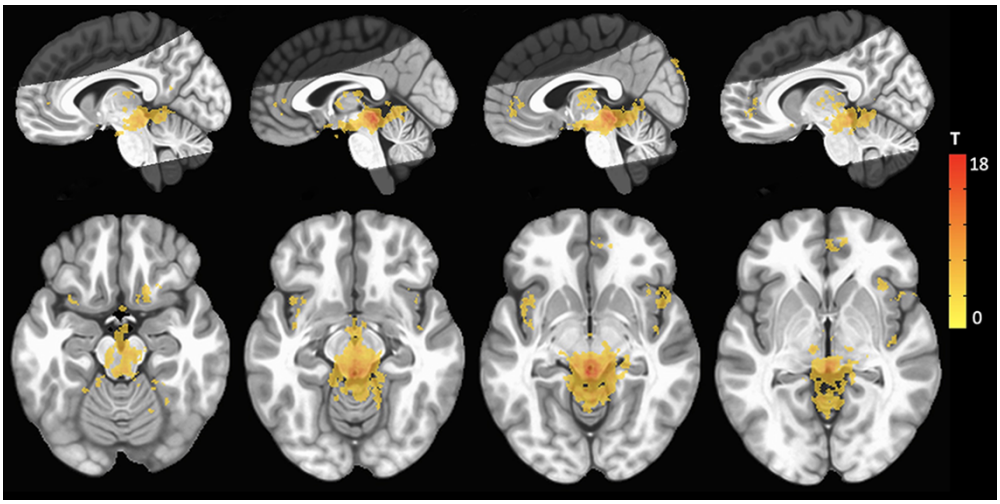

Fig. 3. Results of voxel-wise functional connectivity using the whole PAG as a seed. Warm-colored clusters indicate regions that show increased connectivity with the PAG. Images are overlaid on a standard MNI template at voxel-wise threshold ($P < 0.001$) and cluster thresholds ($P < 0.05$, $k > 303$). Bright gray regions indicate average coverage of the axial partial acquisition functional scan.

and brain stem regions (see Table 1 for complete list of significant clusters).

PAG column functional connectivity Results of the ANCOVA comparing voxel-wise resting state functional connectivity of the four PAG columns showed there were no clusters that survived correction for multiple comparisons in the overall column factor (voxel-wise $P < 0.001$, cluster-wise $P < 0.05$, $k > 303$), although further examination of the main effect terms for each column revealed significant clusters. However, since the overall column factor in the ANCOVA did not yield any results that survived correction, the results from the main effects of each column are relegated to the supplement (Supplementary Table S3). Exploration of post-hoc pairwise comparisons of column functional connectivity maps further demonstrated no differences between any two pairs of columns. Individual column effects were, thus, only apparent after controlling for the effects of all three other columns. In light of these null findings, to ensure the analytic methods employed work more generally, a positive control analysis was conducted using another midbrain region, the ventral tegmental area (VTA), which has well-established connectivity patterns in the literature. Results suggest VTA resting-state connectivity was as expected (Supplementary Table S4 and Supplementary Figure S4), providing evidence that the analytic approach employed within the current study was effective and appropriate. As mentioned previously, the correlation of time series between pairwise comparisons of PAG columns showed high correlations among all pairs of columns. High correlations of activity among

Table 1. Coordinates of peak voxels for whole PAG functional connectivity

	Peak coordinates				
	X	Y	Z	T	k
Brain stem	−0.8	−34.5	−9	17.72	48 200
Right insula	43.5	21	1.5	5.71	3098
Right anterior cingulate	6	48.8	−6.8	6.35	2732
Left insula	−41.2	12.8	−9	6.82	1845
Right superior orbital gyrus	15	18	−19.5	5.72	1003
Left calcarine gyrus	−13.5	−59.2	17.2	4.62	692
Left thalamus	−10.5	−18	−3.8	5.63	503
Left cuneus	3	−87	39	5.38	478
Left cerebellar cortex	−26.2	−45	−21	6.00	377
Right insula	42	−12	−3	5.24	348
Left fusiform	−24.8	−29.2	−27	5.45	316
Left superior temporal gyrus	−50.2	−30	16.5	4.44	310

Voxel-wise threshold $P < 0.001$, cluster threshold $k > 303$. T, t-statistic, k, number of voxels.

columns, close spatial proximity and the absence of threat during rest may explain the lack of differential resting state functional connectivity assessed in pairwise comparisons.

Experiment 1 discussion

The current study utilized high-resolution 7-Tesla MRI to characterize the functional connectivity of the PAG and its columns in healthy individuals at rest. Results indicated the PAG did not show differential connectivity within its columns during rest, although whole PAG functional connectivity was in theoretically expected regions within the limited field of view examined.

Previous work in nonhuman animal models has demonstrated functional differences in the PAG columns that has been replicated in humans under various task paradigms (Mobbs *et al.*, 2007; Hahn *et al.*, 2013; Ritter *et al.*, 2013; Satpute *et al.*, 2013; Faull *et al.*, 2015, 2016; Faull and Pattinson, 2017; Hashemi *et al.*, 2019; Kragel *et al.*, 2019). However, at rest, the current study did not find any functional connectivity differences between PAG columns across the brain within the field of view examined. While these results are inconsistent with previous work (Coulombe *et al.*, 2016; Faull and Pattinson, 2017), despite similar sample sizes and characteristics, there are a few methodological differences to note. First, Faull and Pattinson (2017) defined PAG columns using functional activation from a breath-holding task, whereas the current study utilized a rigorous manual tracing protocol based on anatomical landmarks. Second, Coulombe *et al.* (2016) not only described PAG column connectivity at 3T, but also used spherical ROIs that greatly reduced spatial precision and separability of PAG columns (Coulombe *et al.*, 2016). These key differences in study methodology and analysis approaches may explain the lack of consensus in specifically PAG column connectivity results. However, results of the voxel-wise functional connectivity analysis using the whole PAG seed are consistent with previous work demonstrating that the PAG is functionally connected to the prefrontal, insular cortices and brain stem gray matter in many human and nonhuman animal models (Mantyh, 1983a,b; An *et al.*, 1998; Jansen *et al.*, 1998; Bandler *et al.*, 2000; Krout and Loewy, 2000; Coulombe *et al.*, 2016; Harricharan *et al.*, 2016; Galgano *et al.*, 2019).

Perhaps PAG column functional differences only emerge when under present threat or in anxiety-like states (Mobbs *et al.*, 2007; Faull *et al.*, 2016; Harricharan *et al.*, 2016; Faull and Pattinson, 2017), but not at rest in healthy individuals. From a theoretical standpoint, the PAG is involved in threat detection and initiation of defensive behaviors, both of which are processes belonging to a larger circuitry underlying fear and anxiety (Fanselow, 1991; Behbehani, 1995; An *et al.*, 1998; Bandler *et al.*, 2000; Lindquist *et al.*, 2012; Sylvester *et al.*, 2012; Harricharan *et al.*, 2016; Motta *et al.*, 2017; Torrisi *et al.*, 2018). However, results of the current study would suggest that while the PAG is critical for fear and anxiety, it may not be 'online' or recruited when there is no imminent threat present (Mobbs *et al.*, 2007). In the resting state scan, participants were simply instructed to lie still and remain awake, and while the scanner may be daunting at first, most participants settle into a comfortable position within minutes. This scenario may simply not be threatening and thus necessitate recruitment of the PAG.

Moreover, we are confident that PAG signal was adequately obtained and proper alignment and extraction of seeds for all participants was ensured. Therefore, we believe the observed results are not due to technical or analytical error. Furthermore, results of the VTA positive control analysis (see Supplementary material) lend support to the appropriate analytic strategy used. Given the clear absence of threat and that the study sample were all neurologically healthy individuals who presumably have 'normal' brain function, the functional roles of the PAG columns may not be differentiated and instead behave as a functional unit at rest. However, scan acquisition parameters likely reduced power to detect columnar connectivity (see Limitations) and thus results warrant replication.

Experiment 2: PAG activity under uncertain threat

As previously mentioned, most of the foundational knowledge of the functional role of the PAG has been described in terms of threat responding, and fear and anxiety behaviors in nonhuman animal models (Fanselow, 1991; Behbehani, 1995; An *et al.*, 1998; Bandler *et al.*, 2000; Molchanov and Guimaraes, 2002; Vianna *et al.*, 2003; Bittencourt *et al.*, 2004; Mendes-Gomes and Nunes-de-souza, 2009; Deng *et al.*, 2016; Motta *et al.*, 2017; Vieira-Rasteli *et al.*, 2018; Faull *et al.*, 2019). In humans, investigation of the PAG has demonstrated differential functional roles of the PAG columns in a variety of studies including voluntary breath holding, breathlessness and conditioned respiratory threat (Faull *et al.*, 2015, 2016), responses to painful electrical stimulation (Hahn *et al.*, 2013), noxious heat (Ritter *et al.*, 2013) and cold (La Cesa *et al.*, 2014), working memory load (Kragel *et al.*, 2019), virtual threat imminence (Mobbs *et al.*, 2007; Hashemi *et al.*, 2019) and passive picture viewing of aversive and neutral images (Satpute *et al.*, 2013).

While the role of the PAG in threat detection and response has been repeatedly demonstrated in conditioning paradigms where threat is predictable, there is limited to no work on the role of the PAG in unpredictable threat. Furthermore, to follow up the null results of PAG column connectivity at rest, we decided to evaluate the functional role of the PAG and its columns with a well-validated threat of shock task comparing certain and uncertain threat.

Method

Uncertain threat task paradigm acquisition

The same participants from the resting state analysis also completed the following uncertain threat task paradigm. Prior to scanning, two electrodes for electrical stimulation were placed on participants' left ankle. A shock work-up procedure was then completed to establish each participants' individual level of shock intensity. Participants were instructed to determine a shock level that was 'painful but tolerable' to ensure adequate aversion to the stimulus. Shocks were administered for 500 ms where applicable during the task. Skin conductance was continuously collected using a BIOPAC System (MP-160) with MR-safe disposable electrodes attached to the index and middle finger of the left hand.

The uncertainty task was modeled directly from the NPU task by Gorka *et al.* (2017) (see Figure 4 for trial and block structure). The task is a block design consisting of three conditions: no shock (N), predictable shock (P) and unpredictable shock (U). There were three runs of the task during which each condition (N/P/U) was presented once per run with order of condition presentation counterbalanced across runs. Order of runs was counterbalanced across participants. Each condition block consisted of six trials lasting a total of 78 s, as such a full run lasted 234 s (93 TRs). Interstimulus intervals within a condition block ranged from 5 to 7 s.

Each trial began with a fixation cross and text at the bottom of the screen serving to remind participants of the current experimental block condition. Following fixation, a variable 8 s countdown was shown. In the N condition, no shocks were delivered at any point in the trial, in the P condition a shock was delivered when the countdown reached 1 and in the U condition a shock was delivered randomly at any point during the countdown. In total, participants received 36 electric shocks across all 3 runs, 18 in the P condition, 18 in the U condition. Participants were not instructed to make any responses during the task.

Uncertain threat (NPU) task paradigm analysis

Preprocessing of the NPU task was done in a similar manner as the resting state. Briefly, the first three volumes were removed from the EPI and remaining volumes were slice time corrected to the first EPI slice. Reverse polarity scans were again used for distortion correction. Functional volumes were then co-registered to the first functional volume and aligned to the anatomy. The anatomy and EPI were then warped to MNI space (MNI152) for group analysis. Again, to preserve the high-resolution EPI and enhance signal within our PAG seed during the task, functional images were minimally smoothed with a 3.6 mm kernel. Six head motion parameters were included as nuisance regressors, and one censor file was included into the regression that excluded TRs where more than 10% of voxels in the brain were outliers and where motion exceeded 0.3 mm. Shock delivery was also modeled in the regression to account for shock-related variability in brain activation. Of the original 57 participants analyzed in the resting state analysis, 35 completed all runs of the task and were retained according to motion and censor thresholds (12 males, 23 females, $M_{age} = 21.71$, $s.d._{age} = 2.78$). BOLD signal was modeled over the course of the full condition block using duration modulated basis functions in AFNI.

First, activation of the PAG between experimental conditions, at the block level, was evaluated in a voxel-wise manner (i.e. across all voxels within the whole PAG irrespective of column delineations) using AFNI's *3dMVM* with sex as a covariate. Given that the average size of the PAG across participants was only ~1100 voxels, a small volume correction (Faull and Pattinson, 2017), using the average group PAG mask in *3dClustSim*, was applied to correct for multiple comparisons (Woo *et al.*, 2014; Chen

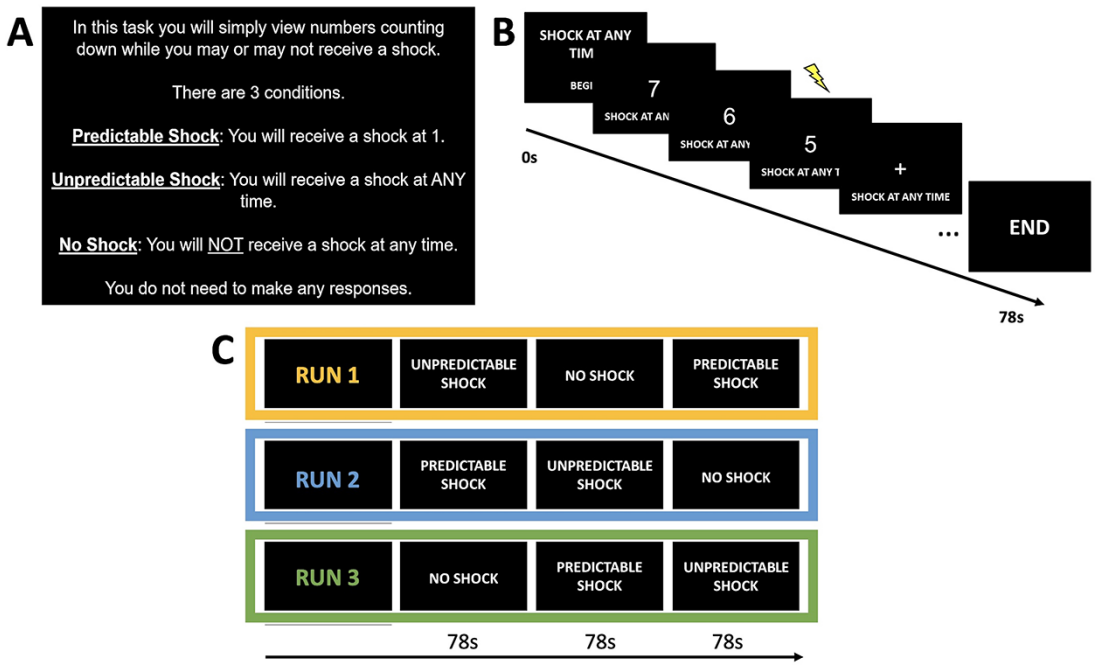

Fig. 4. (A) Instruction screen presented to participants at the beginning of each experimental run. (B) Schematic of example trial structure for an unpredictable (U) trial. (C) Structure of task runs. Each run consisted of 1 block of each condition. Order of condition presentation across runs was counterbalanced. Order of runs was counterbalanced across participants.

et al., 2017). Furthermore, for all NPU analyses, unless otherwise stated, we opted to use a more liberal voxel-wise threshold (voxel-wise: $P < 0.01$, cluster: $P < 0.05$, $k > 47$).

Next, to compare voxel-wise PAG activation within columns across experimental conditions, voxel-wise contrasts were evaluated for each of the four PAG columns in separate ANCOVA's, using AFNI's *3dMVM* with sex as a covariate. In addition, average beta weights for each participant for each column were compared across conditions using repeated measures analyses of variance (ANOVAs). To examine fluctuations in activation, time series data from each column were also extracted, averaged across participants and plotted by condition.

For completeness, average whole PAG and whole brain activity were compared across conditions although details and results of these analyses are reported in the Supplementary material.

Results

Uncertain threat task results

Analysis of skin conductance level is described in the Supplementary material. At the block level, results of a one-way repeated measures ANOVA showed an effect of experimental condition on the skin conductance level such that participants had significantly higher skin conductance levels during U blocks compared to P, with marginal effects of U > N and P > N (Supplementary Figure S5). These results affirm the validity of the NPU paradigm (Gorka et al., 2017).

Voxel-wise whole PAG

No clusters survived correction for any condition comparisons in the voxel-wise activation analysis within the whole PAG mask. However, further examination showed greater activation for U > P for two small clusters within the right ventrolateral and lateral columns that just missed the cluster-size threshold ($P < 0.05$, $k > 47$; Figure 5). The rostral cluster (MNI coordinates: 1.5, 27.8 and −3.8) lies primarily in the right ventrolateral column with some overlap in the right lateral column ($t = 3.19$, $k = 25$). The caudal cluster (MNI coordinates: 3, 31.5 and −10.5), bridges both right ventrolateral and lateral columns evenly ($t = 3.09$, $k = 15$). No other clusters showed marginal effects for U vs. N or P vs. N.

Voxel-wise PAG columns

Results of the separate PAG column ANCOVAs showed no significant voxels in the overall task condition factor that survived correction for any of the four columns. Therefore, there were no voxel-wise activation differences within individual columns for any task condition comparisons. However, average beta weights for each participant for each column were compared using repeated measures ANOVAs (Figure 6). Results of this analysis indicate a significant effect of column during P blocks ($F(1.41, 47.86) = 4.46$, $P = 0.02$) such that the dorsolateral column showed greater activation than ventrolateral ($t(35) = 27$, $p_{Holm} = 0.01$). In addition, there was a significant effect of condition within the ventrolateral column ($F(2, 68) = 3.01$, $P = 0.05$) such that there was greater activation during U compared to P blocks although this effect did not survive correction for multiple comparisons ($t(35) = 27$, $p_{uncorrected} = 0.09$). Examination of time series data by column across all runs for each condition shows no clear differentiation of PAG column activity for any condition (Figure 6). As reported in the supplement, the whole PAG also showed no clear differences in average activation (Supplementary Table S5) or pattern of activation in time series plots across conditions (Supplementary Figure S6). Despite these largely null findings, there were other expected brain regions, beyond the PAG, that showed robust activation to each condition as well as differential activation between conditions (Supplementary Figure S7, Supplementary Table S6), evidence of the validity of the NPU task in regions other than the PAG.

Experiment 2 discussion

Given the lack of robust results from the resting state analysis, we were keen on investigating PAG activity in our sample to certain and uncertain threat of shock. Despite a strong rationale for expecting PAG engagement in response to threat, results did not turn out as expected. At the block level, although there were marginal effects in the voxel-wise analysis of the whole PAG and in the comparison of average beta weights within PAG columns, there were no robust activity differences within the PAG columns or in the PAG as a whole. In addition, an examination of the time course of PAG activity did not show any meaningful patterns of transient activity in the PAG columns or in the whole PAG over the course of the task.

Although marginal, the current results suggest that there is some degree of activation in the PAG in response to uncertain threat. For U compared to P, greater activation at the voxel level along the ventrolateral column as well as greater average ventrolateral column activity suggests that there may be something unique to the function of the ventrolateral PAG in humans in response to uncertain threat. These results broadly correspond with the results in Satpute et al. (2013) that showed similar activation to aversive image viewing in small clusters of the lateral and ventrolateral columns. Although there are clear differences between aversive image viewing and threat of shock paradigms, the concordance of activation in similar regions to threatening stimuli suggests the lack of robust results in the current study may simply be due to reduced power (see Limitations) or, from a conceptual standpoint, that PAG involvement in specifically uncertain threat is more nuanced. Nonetheless, the lack of robust task activation differences was rather surprising, as such we offer up a few potential explanations.

While the PAG has been previously shown to play a role in the initiation of fear-related behaviors, it is possible it may not play a role in perception or appraisal of uncertainty (Aupperle and Paulus, 2010; Drabant et al., 2011; Grupe and Nitschke, 2013; Harricharan et al., 2016). Neuroimaging studies of uncertainty have shown notable activity of the amygdala (Herry et al., 2007; Sarinopoulos et al., 2010; Alvarez et al., 2011; Janak and Tye, 2015; Herrmann et al., 2016; Torrisi et al., 2018), ACC (Shankman et al., 2014; Alvarez et al., 2015; Herrmann et al., 2016), ventromedial PFC (Aupperle and Paulus, 2010; Herrmann et al., 2016), BNST (Alvarez et al., 2011, 2015; Herrmann et al., 2016; Torrisi et al., 2018) and insula (Aupperle and Paulus, 2010; Sarinopoulos et al., 2010; Shankman et al., 2014) in response to various uncertain stimuli and periods of anticipation. This body of literature has suggested that uncertainty may 'prime' the fear system to over-respond to the threat stimulus. The results of the voxel-wise contrasts within the limited field of view across NPU conditions lend support to this theory by demonstrating recruitment of regions beyond the PAG in each of the experimental conditions. Most notable of these results was the robust activation of the insula and caudate in response to unpredictable compared to predictable threat of shock.

While there is a reasonable explanation for the lack of PAG activity during the uncertain condition, it is also surprising that PAG activity did not emerge in response to the predictable threat condition. A fair amount of work has detailed the PAG's response to threat (Mobbs et al., 2007; Hahn et al., 2013; Ritter et al., 2013;

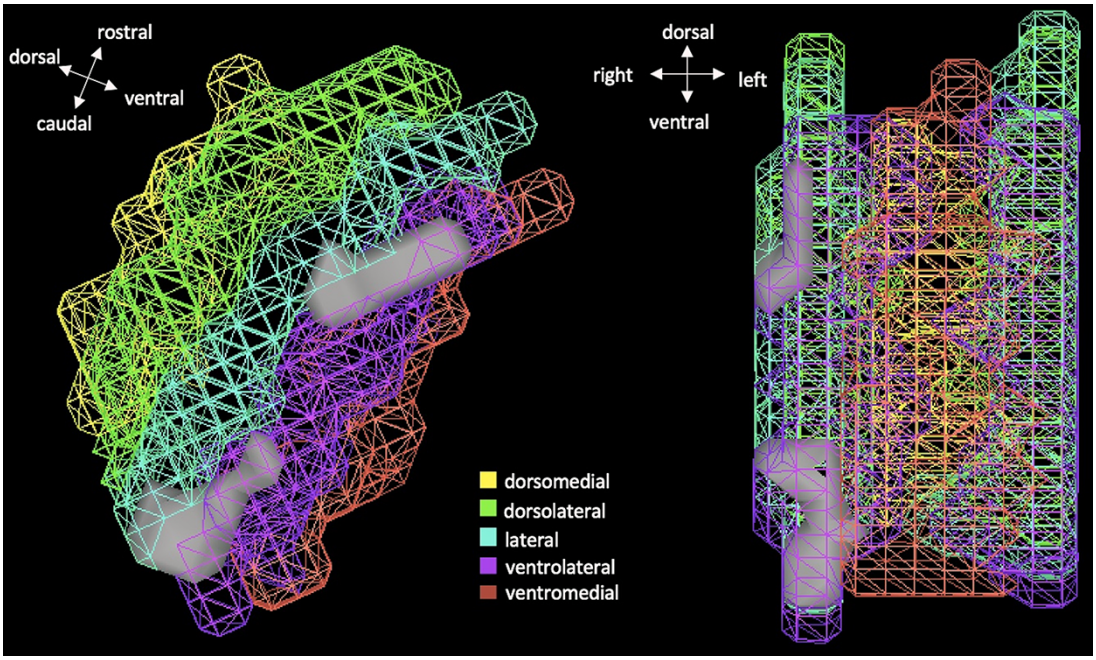

Fig. 5. Two marginally significant clusters showing greater activation during U block compared to P. Clusters are marginal at the following thresholds ($P < 0.01$, $k > 47$ corrected). Note, the image depicts PAG columns, but this is only a means to orient spatial location of the significant clusters (gray). Indeed, the voxel-wise analysis was run with all voxels in the whole PAG seed.

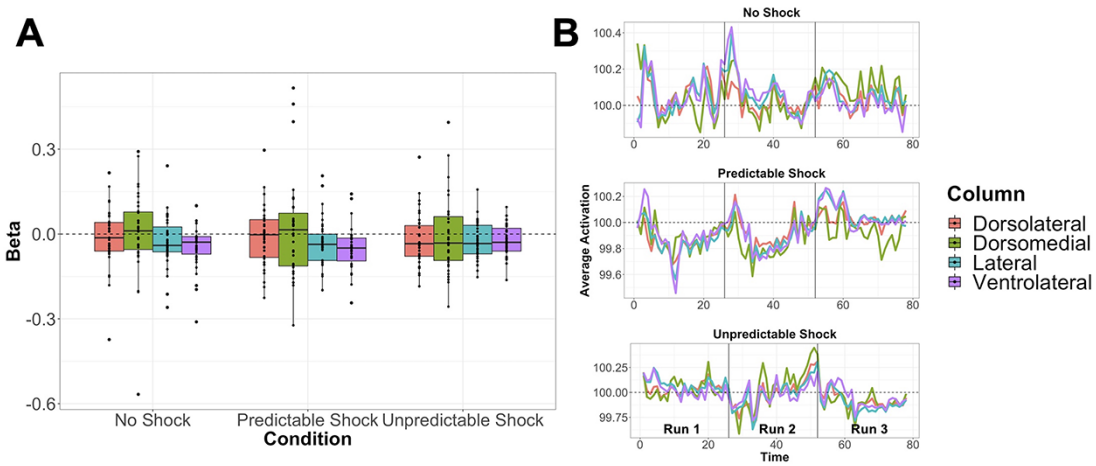

Fig. 6. (A) Average activation (beta) by condition and PAG column. Black dots represent individuals, boxplots designate mean values and interquartile ranges. Results of repeated measures ANOVAs show the dorsolateral column had greater activation than ventrolateral during P blocks, and a marginal effect within the ventrolateral column such that there was greater activation during U compared to P blocks. (B) Average time series of activation by column for each condition. All runs are concatenated separated by vertical black lines. Time series plots show no clear differentiation in PAG activation by condition.

Satpute *et al.*, 2013; La Cesa *et al.*, 2014; Faull *et al.*, 2015, 2016; Faull and Pattinson, 2017; Hashemi *et al.*, 2019; Kragel *et al.*, 2019); however, a notable difference between this body of work and the current study is the use of the temporal countdown ahead of the threat presentation. This period of time was explicit and directed. Predictable threat or not, the countdown introduces an element of anticipation that has not been clearly examined with regard to the PAG. The anticipation period may impede a clear response from the PAG due to the recruitment of regions, as demonstrated in the whole brain voxel-wise contrasts (Supplementary Table S4), including the insula, ACC, PFC and hippocampus that in the literature have more theoretical relevance to anticipation (Herry *et al.*, 2007; Aupperle and Paulus, 2010; Sarinopoulos *et al.*, 2010; Alvarez *et al.*, 2011, 2015; Shankman *et al.*, 2014; Herrmann *et al.*, 2016; Torrisi *et al.*, 2018).

At its core, the NPU task is one aimed to understand the effects of uncertainty rather than the effects of threat or fear (Gorka *et al.*, 2017). While these concepts can be hard to disentangle definitively, the point is the PAG may not be recruited during the current NPU task because it is not involved in the network of regions responsive to uncertainty or anticipation such as the amygdala, ACC, vmPFC and BNST, (Aupperle and Paulus, 2010; Drabant *et al.*, 2011; Grupe and Nitschke, 2013; Janak and Tye, 2015; Torrisi *et al.*, 2018). This explanation is likely too nuanced in the true effects at play here but may serve as one potential theory to follow up in future studies. Given the lack of robust results in the resting

state analysis, the lack of results in the NPU task should be more thoroughly explored before discounting the PAG's involvement in anticipation of threatening stimulus as there may be some inherent biases unique to the current study or sample. Nevertheless, our confidence in the validity of the null findings is increased due to the rigorous analytic approach employed to ensure results were not artifacts.

Limitations

The current study is not without limitation. Most notably, the current study only had partial coverage of the brain for the functional MRI acquisition. As 7-Tesla MRI is well known to be susceptible to increased artifact and distortion, the decision was made for partial acquisition to optimize the signal and resolution from the regions of greatest interest to the current study. However, given the limited range of functional acquisition, our reported results of voxel-wise resting state functional connectivity with the PAG may not represent the full connectivity results. Furthermore, the power to detect connectivity and activity was significantly reduced due to a combination of factors including the partial spatial acquisition, the signal reduction afforded to voxels <1 mm and the positioning and thickness of slices not specifically tailored to optimize PAG column signal. Moreover, despite careful preprocessing and analysis, the whole brain functional connectivity analyses should be interpreted with caution as results indicated connectivity in orbitofrontal regions and across distributed brain stem gray matter, regions in the field of view that typically exhibit dropout at ultra-high resolution (see Supplementary Figure S3 for average FOV in the current sample). In addition, there are a few limitations to hand-drawing the PAG as done in the current study, rather than using previously derived masks, that include bias in implementing the drawing protocol and margins for error when drawing from subject to subject. However, manual tracing at the individual level and back projection of the group-level PAG columns to individuals was rigorously checked for each participant.

There were also a few notable limitations to the design of the overall study. The NPU task as described accompanied two other tasks in the scanner that were part of a larger study. These tasks also used shock as a learning contingent in their respective paradigms, and the order of the task administration was counterbalanced across participants. This means, the NPU task did not standalone as the sole task with shock as a potential aversive stimulus and was not always the first task participants experienced. Having the additional tasks during the scan session, which were beyond the scope of the current study, may have led to a habituation of the uncertain threat in the NPU task making the overall experimental paradigm less salient. In addition, while initially the presentation of the electric shock for some individuals is aversive, most participants anecdotally report it as only mildly aversive by the end of the scan session suggesting clear habituation to its presentation (Klormon, 1974). The combination of these factors and the shock presentation only being a quick 500 ms together may not prove to be very threatening (Klormon, 1974; Shankman *et al.*, 2011). Thus, the PAG may not be recruited under these conditions or at least may need a higher threat threshold to initiate any defensive behaviors despite the uncertainty of threat within the experimental paradigm.

General conclusion

Despite the limitations the results of the current study are still rather interesting. At rest and in healthy individuals, there are no differences in the voxel-wise functional connectivity patterns of the PAG's columns. In addition, there were no robust differences of PAG activity in response to predictable and unpredictable threat suggesting that the PAG may not play a role in processing uncertain threat. The results of the current study suggest nuances within the role of the PAG, including rest and threat paradigms in which the PAG is not responsive, that have not been described previously. The continuation of PAG research in healthy individuals is important for the understanding of the PAG's role in anxiety neurocircuitry.

Acknowledgement

This work would not be possible without the incredible team of scan technicians, engineers and physicists at the Center for Imaging Research at MCW.

Funding

The current work was supported by the Daniel M. Soref Charitable Trust through the Center for Imaging Research at the Medical College of Wisconsin.

Ethics and integrity statements

None of the authors have any potential conflicts of interest to disclose. The data are not available for sharing at this time, but we are working with the IRB to explore potential options for sharing. All procedures were approved and overseen by the University of Wisconsin—Milwaukee and Medical College of Wisconsin Institutional Review Boards, and written consent was obtained from all participants.

Conflict of interest

The authors declare no conflicts of interest, financial or otherwise, related to the authorship or publication of this manuscript.

Supplementary data

Supplementary data are available at SCAN online.

References

Alvarez, R.P., Chen, G., Bodurka, J., Kaplan, R., Grillon, C. (2011). Phasic and sustained fear in humans elicits distinct patterns of brain activity. *NeuroImage*, **55**(1), 389–400.

Alvarez, R.P., Kirlic, N., Misaki, M., *et al.* (2015). Increased anterior insula activity in anxious individuals is linked to diminished perceived control. *Translational Psychiatry*, **5**(6), e591.

An, X., Bandler, R., Ongur, D., Price, J.L. (1998). Prefrontal cortical projections to longitudinal columns in the midbrain periaqueductal gray in macaque monkeys. *The Journal of Comparative Neurology*, **401**(4), 455–79.

Aupperle, R.L., Paulus, M.P. (2010). Neural systems underlying approach and avoidance in anxiety disorders. *Dialogues in Clinical Neuroscience*, **12**(4), 517–31.

Bandler, R., Keay, K.A., Floyd, N., Price, J. (2000). Central circuits mediating patterned autonomic activity during active vs. passive emotional coping. *Brain Research Bulletin*, **53**(1), 95–104.

Barbaresi, P., Mensa, E. (2016). Connections from the rat dorsal column nuclei (DCN) to the periaqueductal gray matter (PAG). *Neuroscience Research*, **109**, 35–47.

Behbehani, M.M. (1995). Functional characteristics of the midbrain periaqueductal gray. *Progress in Neurobiology*, **46**(6), 575–605.

Bittencourt, A.S., Carobrez, A.P., Zamprogno, L.P., Tufik, S., Schenberg, L.C. (2004). Organization of single components of defensive behaviors within distinct columns of periaqueductal gray matter of the rat: role of N-methyl-D-aspartic acid glutamate receptors. *Neuroscience*, **125**(1), 71–89.

Chen, G., Adleman, N.E., Saad, Z.S., Leibenluft, E., Cox, R.W. (2014). Applications of multivariate modeling to neuroimaging group analysis: a comprehensive alternative to univariate general linear model. *NeuroImage*, **99**, 571–88.

Chen, X., Lu, B., Yan, C.-G. (2017). Reproducibility of R-fMRI metrics on the impact of different strategies for multiple comparison correction and sample sizes. *Neuroscience*, **99**, 571–88.

Coulombe, M.-A., Erpelding, N., Kucyi, A., Davis, K.D. (2016). Intrinsic functional connectivity of periaqueductal gray subregions in humans. *Human Brain Mapping*, **37**(4), 1514–30.

Cox, R.W. (1996). AFNI: software for analysis and visualization of functional magnetic resonance neuroimages. *Computers and Biomedical Research, an International Journal*, **29**(3), 162–73.

Deng, H., Xiao, X., Wang, Z. (2016). Periaqueductal gray neuronal activities underlie different aspects of defensive behaviors. *The Journal of Neuroscience*, **36**(29), 7580–8.

Drabant, E.M., Kuo, J.R., Ramel, W., *et al.* (2011). Experiential, autonomic, and neural responses during threat anticipation vary as a function of threat intensity and neuroticism. *NeuroImage*, **55**(1), 401–10.

Duvernoy, H. (2009). *Internal Architecture of the Brain Stem with Key Axial Section*. Vienna: Springer, 53–93.

Ezra, M., Faull, O.K., Jbabdi, S., Pattinson, K.T. (2015). Connectivity-based segmentation of the periaqueductal gray matter in human with brainstem optimized diffusion MRI. *Human Brain Mapping*, **36**(9), 3459–71.

Fanselow, M. (1991). *The Midbrain Periaqueductal Gray as a Coordinator of Action in Response to Fear and Anxiety* (Depaulis, A., Bandler, R., editors). Boston, MA: Springer, 151–73.

Faull, O.K., Jenkinson, M., Clare, S., Pattinson, K.T. (2015). Functional subdivision of the human periaqueductal grey in respiratory control using 7 Tesla fMRI. *NeuroImage*, **113**, 356–64.

Faull, O.K., Jenkinson, M., Ezra, M., Pattinson, K.T. (2016). Conditioned respiratory threat in the subdivisions of the human periaqueductal gray. *eLife*, **5**, e12047.

Faull, O.K., Subramanian, H.H., Ezra, M., Pattinson, K.T.S. (2019). The midbrain periaqueductal gray as an integrative and interoceptive neural structure for breathing. *Neuroscience and Biobehavioral Reviews*, **98**, 135–44.

Faull, O.K., Pattinson, K.T. (2017). The cortical connectivity of the periaqueductal gray and the conditioned response to the threat of breathlessness. *eLife*, **6**, e21749.

Fischl, B. (2012). FreeSurfer. *NeuroImage*, **62**(2), 774–81.

Galgano, J., Pantazatos, S., Allen, K., Yanagihara, T., Hirsch, J. (2019). Functional connectivity of PAG with core limbic system and laryngeal cortico-motor structures during human phonation. *Brain Research*, **1707**, 184–9.

Gorka, S.M., Lieberman, L., Shankman, S.A., Phan, K.L. (2017). Startle potentiation to uncertain threat as a psychophysiological indicator of fear-based psychopathology: an examination across multiple internalizing disorders. *Journal of Abnormal Psychology*, **126**(1), 8–18.

Grupe, D.W., Nitschke, J.B. (2013). Uncertainty and anticipation in anxiety: an integrated neurobiological and psychological perspective. *Nature Reviews Neuroscience*, **14**(7), 488–501.

Hahn, A., Kranz, G.S., Seidel, E.M., *et al.* (2013). Comparing neural response to painful electrical stimulation with functional MRI at 3 and 7 T. *NeuroImage*, **82**, 336–43.

Harricharan, S., Rabellino, D., Frewen, P.A., *et al.* (2016). FMRI functional connectivity of the periaqueductal gray in PTSD and its dissociative subtype. *Brain and Behavior*, **6**(12), e00579.

Harris, J.J., Reynell, C. (2017). How do antidepressants influence the BOLD signal in the developing brain? *Developmental Cognitive Neuroscience*, **25**, 45–57.

Hashemi, M.M., Gladwin, T.E., Valk, N.M.D., *et al.* (2019). Neural dynamics of shooting decisions and the switch from freeze to fight. *Scientific Reports*, **9**(1), 4240–8.

Herrmann, M.J., Boehme, S., Becker, M.P.I., *et al.* (2016). Phasic and sustained brain responses in the amygdala and the bed nucleus of the stria terminalis during threat anticipation. *Human Brain Mapping*, **37**(3), 1091–102.

Herry, C., Bach, D.R., Esposito, F., *et al.* (2007). Processing of temporal unpredictability in human and animal amygdala. *Journal of Neuroscience*, **27**(22), 5958–66.

Janak, P.H., Tye, K.M. (2015). From circuits to behaviour in the amygdala. *Nature*, **517**(7534), 284–92.

Jansen, A.S.P., Farkas, E., Sams, J.M., Loewy, A.D. (1998). Local connections between the columns of the periaqueductal gray matter: a case for intrinsic neuromodulation. *Brain Research*, **784**(1–2), 329–39.

Jo, H.J., Saad, Z.S., Simmons, W.K., Milbury, L.A., Cox, R.W. (2010). Mapping sources of correlation in resting state FMRI, with artifact detection and removal. *NeuroImage*, **52**(2), 571–82.

Klormon, R. (1974). Habituation of fear: effects of intensity and stimulus order. *Psychophysiology*, **11**(1), 15–26.

Kragel, P.A., Bianciardi, M., Hartley, L., *et al.* (2019). Functional involvement of human periaqueductal gray and other midbrain nuclei in cognitive control. *The Journal of Neuroscience*, **39**(31), 6180–9.

Krout, K.E., Loewy, A.D. (2000). Periaqueductal gray matter projections to midline and intralaminar thalamic nuclei of the rat. *The Journal of Comparative Neurology*, **424**(1), 111–41.

La Cesa, S., Tinelli, E., Toschi, N., *et al.* (2014). FMRI pain activation in the periaqueductal gray in healthy volunteers during the cold pressor test. *Magnetic Resonance Imaging*, **32**(3), 236–40.

Lindquist, K.A., Wager, T.D., Kober, H., Bliss-Moreau, E., Barrett, L.F. (2012). The brain basis of emotion: a meta-analytic review. *The Behavioral and Brain Sciences*, **35**(3), 121–43.

Mantyh, P.W. (1983a). Connections of midbrain periaqueductal gray in the monkey. I. Ascending efferent projections. *Journal of Neurophysiology*, **49**(3), 567–81.

Mantyh, P.W. (1983b). Connections of midbrain periaqueductal gray in the monkey. II. Descending efferent projections. *Journal of Neurophysiology*, **49**(3), 582–94.

Menant, O., Andersson, F., Zelena, D., Chaillou, E. (2016). The benefits of magnetic resonance imaging methods to extend the knowledge of the anatomical organisation of the periaqueductal gray in mammals. *Journal of Chemical Neuroanatomy*, **77**, 110–20.

Mendes-Gomes, J., Nunes-de-souza, R.L. (2009). Anxiolytic-like effects produced by bilateral lesion of the periaqueductal gray in mice: influence of concurrent nociceptive stimulation. *Behavioural Brain Research*, **203**(2), 180–7.

Mobbs, D., Petrovic, P., Marchant, J.L., *et al.* (2007). When fear is near: threat imminence elicits prefrontal-periaqueductal gray shifts in humans. *Science*, **317**(5841), 1079–83.

Molchanov, M.L., Guimaraes, F.S. (2002). Anxiolytic-like effects of AP7 injected into the dorsolateral or ventrolateral columns of the periaqueductal gray of rats. *Psychopharmacology*, **160**(1), 30–8.

Motta, S.C., Carobrez, A.P., Canteras, N.S. (2017). The periaqueductal gray and primal emotional processing critical to influence complex defensive responses, fear learning and reward seeking. *Neuroscience and Biobehavioral Reviews*, **76**(Pt A), 39–47.

Ritter, A., Franz, M., Dietrich, C., Miltner, W.H., Weiss, T. (2013). Human brain stem structures respond differentially to noxious heat. *Frontiers in Human Neuroscience*, **7**, 530.

Sarinopoulos, I., Grupe, D.W., Mackiewicz, K.L., *et al.* (2010). Uncertainty during anticipation modulates neural responses to aversion in human insula and amygdala. *Cerebral Cortex*, **20**(4), 929–40.

Satpute, A.B., Wager, T.D., Cohen-Adad, J., *et al.* (2013). Identification of discrete functional subregions of the human periaqueductal gray. *Proceedings of the National Academy of Sciences of the United States of America*, **110**(42), 17101–6.

Shankman, S., Gorka, S., Nelson, B., Fitzgerald, D., Phan, K., O'Daly, O. (2014). Anterior insula responds to temporally unpredictable aversiveness: an fMRI study. *NeuroReport*, **25**(8), 596–600.

Shankman, S.A., Robison-Andrew, E.J., Nelson, B.D., Altman, S.E., Campbell, M.L. (2011). Effects of predictability of shock timing and intensity on aversive responses. *International Journal of Psychophysiology*, **80**(2), 112–8.

Sylvester, C.M., Corbetta, M., Raichle, M.E., *et al.* (2012). Functional network dysfunction in anxiety and anxiety disorders. *Trends in Neurosciences*, **35**(9), 527–35.

Torrisi, S., Gorka, A.X., Gonzalez-Castillo, J., *et al.* (2018). Extended amygdala connectivity changes during sustained shock anticipation. *Translational Psychiatry*, **8**(1), 33–6.

Torrisi, S., O'Connell, K., Davis, A., *et al.* (2015). Resting state connectivity of the bed nucleus of the stria terminalis at ultra-high field. *Human Brain Mapping*, **36**(10), 4076–88.

Vianna, D.M., Borelli, K.G., Ferreira-Netto, C., Macedo, C.E., Brandao, M.L. (2003). Fos-like immunoreactive neurons following electrical stimulation of the dorsal periaqueductal gray at freezing and escape thresholds. *Brain Research Bulletin*, **62**(3), 179–89.

Vieira-Rasteli, E.B., de Paula, B.B., de Paiva, Y.B., Coimbra, N.C., Leite-Panissi, C.R.A. (2018). Restricted lesions of the ventrolateral or dorsal columns of the periaqueductal gray promotes distinct effects on tonic immobility defensive analgesia in guinea pigs. *Physiology & Behavior*, **194**, 538–44.

Weis, C.N., Huggins, A.A., Bennett, K.P., Parisi, E.A., Larson, C.L. (2019). High-resolution resting-state functional connectivity of the extended amygdala. *Brain Connectivity*, **9**(8), 627–37.

Woo, C.-W., Krishnan, A., Wager, T.D. (2014). Cluster-extent based thresholding in fMRI analyses: pitfalls and recommendations. *NeuroImage*, **91**, 412–9.